Journal of Alloys and Compounds 945 (2023) 169321

Contents lists available at ScienceDirect

Journal of Alloys and Compounds

journal homepage: www.elsevier.com/locate/jalcom

# Can electric heating replace contact heating in high-temperature test for nickel base single crystal superalloy?

Zhen Wang [a,b], Xingzhi Huang [a], Xuan Ye [c], Chong Zhao [a], Jianqiao Hu [b], Zhigang Li [a], Xiaoming Liu [b], Xide Li [a,*]

[a] Department of Engineering Mechanics, Tsinghua University, Beijing 100084, China
[b] State Key Laboratory for Nonlinear Mechanics (LNM), Institute of Mechanics, Chinese Academy of Sciences, Beijing 100190, China
[c] Institute of Nuclear and New Energy Technology, Tsinghua University, Beijing 100084, China

ARTICLE INFO

*Article history:*
Received 4 December 2022
Received in revised form 9 February 2023
Accepted 15 February 2023
Available online 17 February 2023

*Keywords:*
Nickel base single crystal superalloy
Electric heating
High temperature mechanical properties
Microstructure analysis
Jolue heat effect

ABSTRACT

Compared with contact heating or environmental heating in high-temperature test, electric heating has the advantage that it can realize in-situ high-temperature heating in SEM. Especially, it can simplify the heating and loading equipment and clearly obtain surface microstructure information of small scale specimens. However, due to the positive feedback characteristic of Joule thermal effect and other electro-induced effects in materials, such as the influence of electromigration and electric field on dislocation motion, etc. the effectiveness of high temperature mechanical properties of materials obtained under electric heating needs further study. In this paper, the tensile properties of nickel-based single crystal superalloy at room temperature to 950 ℃ were conducted using by electric heating and contact heating modes. The results show that when the heating temperature is below 600 ℃, the fracture mode and dislocation evolution of nickel base single crystal superalloy do not change significantly under two heating modes; When the heating temperature exceeds 600 ℃, the macroscopic mechanical properties change gradually, but the elastic modulus has no obvious difference. Through the distribution of two-phase elements, it is found that the relevant differences are mainly related to element migration. In addition to the thermal effect caused by electric current, the athermal effect promotes dislocation movement and element migration, which leads to the increasing difference of mechanical properties at high temperature under the two heating modes. These results show that at the temperature exceeds 600 ℃, the electric heating method is no longer suitable for studying the high-temperature mechanical properties of nickel-based single crystal superalloy.



## 1. Introduction

Increasing temperature at the inlet and outlet of a gas turbine can improve its work efficiency, and corresponds to stringent requirements for the service temperature of blade materials. Nickel-based single crystal (NBSC) superalloy is widely used for gas turbine blades because of its excellent high-temperature (> 800 °C) mechanical properties [1]. Therefore, in order to better study its high-temperature mechanical properties, researchers have carried out a lot of experimental studies, such as tensile [2,3], creep and fatigue [4–6]. However, it is difficult to establish a physical-based constitutive model due to the lack of microstructure evolution information in macroscopic high-temperature mechanical properties testing. More recently, in-situ small-scale experimental technology was developed to observe the microstructure evolution (voids, slip lines, and dislocations) in real time in the optical microscopy [7], scanning electron microscopy (SEM) [8,9] and transmission electron microscopy (TEM]) [10]. However, in the microscopic environment, how to realize the small-scale heating and ensure that the microstructure characteristics are clearly observed is still the bottleneck restricting the in-situ high-temperature experimental test of NBSC superalloy.

For a long time, researchers have used macro-scale experiments to evaluate the high-temperature mechanical properties of NSBC superalloys, and obtained some consensus [11–15]: (1) the yield stress does not substantially change with increasing temperature in the low-temperature region (room temperature to 600 °C); (2) in the medium-temperature region (600–800 °C), the yield stress increases (which is the abnormal behavior) with increasing temperature; and (3) in the high-temperature region (> 800 °C), the yield stress decreases rapidly with increasing temperature. Meanwhile, the

* Corresponding author.
*E-mail address:* lixide@tsinghua.edu.cn (X. Li).

https://doi.org/10.1016/j.jallcom.2023.169321
0925-8388/

subsequent fractography analysis shows that a/2 < 110 > dislocations cut into the γ′ phase by adopting two modes: dislocation pair coupling antiphase boundary (APB), and dislocation in the form of stacking faults (SFs) that shear the γ′ phase in the low- and medium-temperature region [13,14]. In the medium- and high-temperature regions, the deformation mechanism is mainly dislocation that bypasses the γ′ phase [15]. Obviously, these macro-scale experiments cannot record the information of small crack propagation, plastic slip, dislocation evolution and other processes, which leads to a lack of in-depth and comprehensive understanding about the deformation failure prediction of NBSC superalloys. Although, the researchers also carried out some in-situ small-scale studies on the mechanical properties of NBSC superalloys at the low temperature environment, and established small crack propagation models [16] and constitutive models including plastic slip and dislocation evolution based on the information of microstructure evolution [17]. However, whether these microstructure-related models are suitable for high-temperature deformation and life prediction of NSBC superalloys is lack of verification. The main reason is that in the microscopic environment, when the heating temperature exceeds 700 ℃ [18], such as irradiation heating in SEM cavity, the microscopic imaging will deteriorate. It has been pointed out that the surface deformation information of NBSC superalloys can not be obtained in high-temperature environment, because the temperature of irradiation heating source is much higher than the specimen's temperature, and its number of hot electrons are far more than the secondary electrons on the specimen surface [19]. In order to improve the imaging quality of high-temperature testing environment, electric heating is introduced into SEM to directly heat small-scale specimens. In our previous research, we found that electric heating can achieve an in-situ heating temperature up to 1400 °C in SEM, and obtain clear images of the specimen surface [20]. Thus, it is suitable for heating small-scale specimens and will be widely used in SEM and TEM [10,20]. However, the effectiveness of electric heating for studying the high-temperature mechanical properties of NBSC superalloys still needs further evaluation.

In fact, as a heating method of nickel-based superalloys, electric heating has also attracted the attention of researchers. Liu et al. used a Gleeble-1500 thermal simulation machine to study the mechanical properties of a K403 nickel-based superalloy at 850–1000 °C [21]. With increasing temperature, the peak stress and yield stress decreased, whereas the elongation increased. They also found that the fracture characteristics changed from quasi-brittle cleavage fracture to inter-granular fracture with increasing temperature, and the dislocation density decreased with increasing temperature. Zhang [22] and Patrick [23] comparatively studied the electric-current-assisted and pure thermal tensile behavior of nickel-based superalloys, and pointed that its macro- and micro-behaviors were different for two heating modes due to local Joule heating effect. Different initial structures of the superalloy will also lead to different decreasing proportions of the yield stress for the Inconel 718 alloy [24]. By studying the microstructure evolution characteristics of cold-deformed nickel-based superalloys, Han et al. found that at a high current density, some parallel dislocation morphologies were evident along the electric current direction [25]. The dislocation configuration is consistent with the results observed by Zhang et al. [22]. They explained that the electric current reduced the activation energy of dislocation motion and facilitated its motion [22,25]. Obviously, the high-temperature mechanical properties and dislocation microstructure deformation behavior under electric heating are different from those under pure thermal heating, such as contact heating. It mainly gives rise to the athermal effect in materials [26], which causes uncertainty in evaluating the high-temperature mechanical properties of NBSC superalloys. However, due to the irreplaceable advantages of electric heating in small-scale high-temperature mechanical testing, it is necessary to systematically understand the reliability of electric heating in studying the mechanical properties and micro-mechanism of NBSC superalloys at different temperatures.

In this work, in-situ tensile tests of a NBSC superalloy were carried out from room temperature to 950 °C by contact and electric heating. First, we compared and analyzed the elastic modulus, yield stress, fracture strength, fracture mode, and microstructure evolution of the NBSC superalloy at various temperatures. Second, By analyzing the dislocation mechansisms, the dependence of yield stress on the temperature under the two heating mode was quantitatively explained. Finally, to understand the difference between the above two headting modes, we particularly analyzed the athermal and local Joule heating effects on the mechanical properties of a NBSC superalloy under electric heating, and gave the reliable temperature range (the local high-temperature effect induced by electrical heating and other degradation effects of electro-induced mechanical properties were ignored) of the NBSC superalloy by electric heating. This work provides an experimental basis for further applications of electric heating to studies of dislocation movement under in-situ TEM.

## 2. Experimental procedures

### 2.1. Material and composition characterization

The alloy material used in the experiments was a first-generation NBSC superalloy which was mainly used for high-pressure turbine blades of large gas turbines. Its nominal composition was summarized in Table 1. The specimen was cut directly from the bulk material. To clearly understand the typical microstructure characteristics of the superalloy, its surface was corroded in a reagent of 4 g $CuSO_4$ + 20 mL HCl + 2 mL $H_2SO_4$ + 20 mL $H_2O$ for 30 s at room temperature. Fig. 1(a) indicated that the ordered $L1_2$ structured gamma prime (γ′) phase was evenly embedded into the disordered face-centered cubic gamma phase (γ) and a small quantity of coarse eutectic (γ′+γ) was also contained in the NBSC superalloy. The chemical compositions in the γ′ and γ phase were analyzed by the Energy Disperse Spectorscopy (EDS) in Fig. 1(b). Table 2 showes the original two-phase elemental contents. The γ′ phase was rich in Al, Ti, and Ta elements, which participated in the precipitation strengthening of the NBSC superalloy. The γ phase contained more Cr, Co, and Mo elements, and mainly participated in the solid solution strengthening [27].

### 2.2. Specimen preparation and experimental equipment

The test pieces were fabricated by electrical discharge machining into a dog-bone shape (0.5 mm thickness; in the Fig. 2). The tensile direction of the specimens was the [001] crystal orientation, and the secondary direction was the [010] orientation. To reduce machining burr and obtain clear surface images, the specimens were mechanically polished with coarse and fine SiC sandpaper until there were no obvious scratches on their front and side surfaces under an optical microscope. Finally, ultrasonic cleaning was carried out in an alcoholic solution.

An in-situ SEM high-temperature platform (SS-550, Shimadzu, Japan) was used, as shown in Fig. 3(a). To study the tensile mechanical properties of the NBSC superalloys over a wide temperature range, a heating device previously reported by the authors was also used [20], as shown in Fig. 3(b). Contact and electric heating were used to carry out the tensile tests of the NBSC superalloy under SEM.

**Table 1**
The nominal composition of the material (wt%).

| Element | Ni | Al | Ti | Ta | Cr | Co | Mo | W | C |
|---|---|---|---|---|---|---|---|---|---|
| Content | Balance | 3.6 | 4.1 | 5.0 | 12.2 | 9.0 | 1.9 | 3.8 | 0.07 |

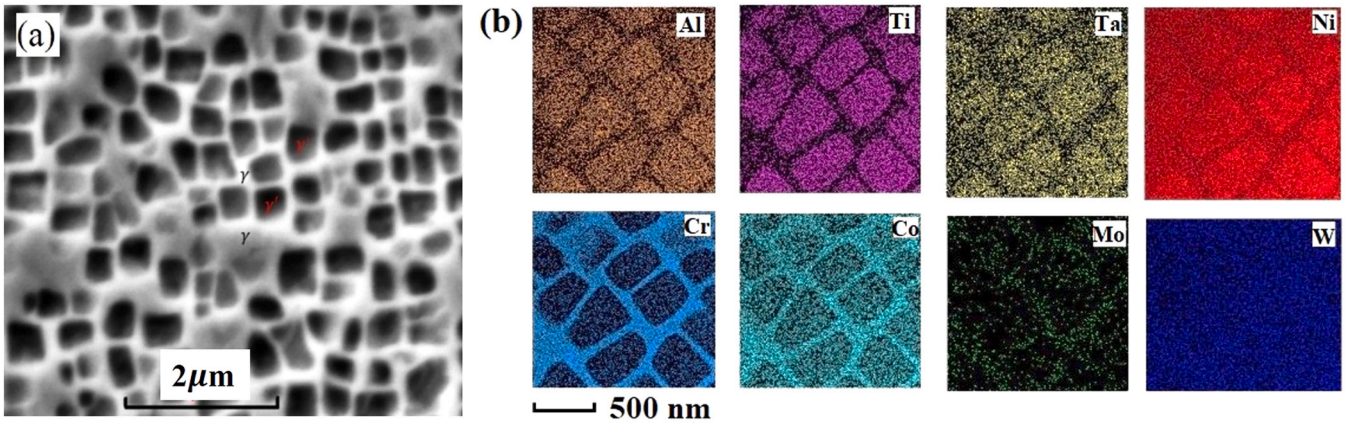


**Fig. 1.** (a) Microstructure of the γ′ and γ phase of the NBSC superalloy, (b) EDS mapping of various chemical compositions.

**Table 2**
Mass percent chemical compositions in the γ′ and γ phases (wt%).

| Element | Ni | Al | Ti | Ta | Cr | Co | Mo | W |
|---|---|---|---|---|---|---|---|---|
| γ′ phase | 69.33 | 5.99 | 6.54 | 6.31 | 2.94 | 5.69 | 0.51 | 2.66 |
| γphase | 51.32 | 2.16 | 1.17 | 1.08 | 23.01 | 12.57 | 3.78 | 4.89 |

The experiments were conducted at room temperature, 600 °C, 800 °C, 950 °C, respectively. The displacement loading rate was 0.001 mm/s. Each specimen was stretched to break.

The temperature consistency of the test specimen by contact heating had been evaluated elsewhere [19]. In addition, to illustrate the temperature distribution in the measurement area of the specimen under electric heating, thermal-electric coupling finite-element simulations were performed. A finite-element model was established in accordance with the size of the specimen. The simulation parameters were from the experimental data of a NBSC superalloy as reported [28,29]. Fig. 3(c) shows the temperature distribution in the intercepted section of the test specimen and the error between the center and both ends was less than 5%, which satisfies the experimental requirements.

### 2.3. Post-test characterization

To compare the tensile fracture characteristics of the NBSC superalloy at various temperatures under the two heating modes, the fracture morphology of each failed specimen was observed by field-emission, high-resolution SEM (Quanta 450, FEI, America). The dislocation structures of the failed specimens were characterized by TEM. The preparation method of TEM thin foils has been described in detail [30]. The dislocation structures under the two heating methods were characterized by bright field imaging by JEM-2100 F field-emission TEM. Because of the influence of elemental diffusion under the two heating modes, TEM-EDS was used to analyze the elemental distribution of the γ and γ′ phases before and after the experiments. There were more than three test positions for each phase to ensure the consistency of the test results.

## 3. Experimental results

### 3.1. Tensile mechanical properties under contact and electric heating

Fig. 4(a) shows the tensile engineering stress–strain curves obtained under the two heating methods at various temperatures for the NBSC superalloy. The solid and dash lines represent contact and electric heating, respectively. First, for contact heating, when the stress exceeded the yield point from room temperature to 800 °C, the sample exhibited strain hardening until the final fracture of the materials. When the temperature was more than 800 °C, the sample mainly exhibited strain softening. However, for the stress–strain curve at 600 °C under electric heating, the sample exhibited strain hardening during the entire tensile process. The slope was slightly less than that under contact heating, which indicated that there was a gradual work hardening effect under electric heating. When the temperature was more than 700 °C, strain hardening occurred first and then strain softening occurred after the yield point. Subsequently, as the temperature increased from 700 °C to 950 °C, the softening behavior was more pronounced and much lower than that of this material at the same temperature by contact heating.

Fig. 4(b)-(d) show the elastic modulus, yield stress, and fracture strength of the NBSC superalloy at various temperatures from the engineering stress–strain curves. The elastic modulus gradually decreased with increasing temperature; the downtrend was more substantial when the temperature was greater than 600 °C, as shown in Fig. 4(b). Researchers have reported this phenomenon in DD11 and CMSX-4 superalloys and found that the main reason was from partial dissolution of the γ′ phase [31,32]. There were no obvious differences in the experimental results of the elastic modulus under the two heating modes. Thus, in the elastic stage, the effect of the electric current on the mechanical properties was mainly attributable to the Joule heat effect. Yield stress is one of the most pertinent parameters in applications of nickel-based superalloys. Regarding contact heating, the yield stress decreased slightly from room temperature to 700 °C; but increased from 700 °C to 800 °C, and decreased sharply when the temperature was greater than 800 °C, as

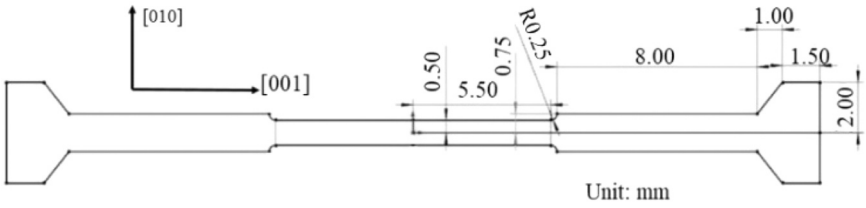


**Fig. 2.** Geometry and crystallographic orientation of the tensile specimen (units: mm).

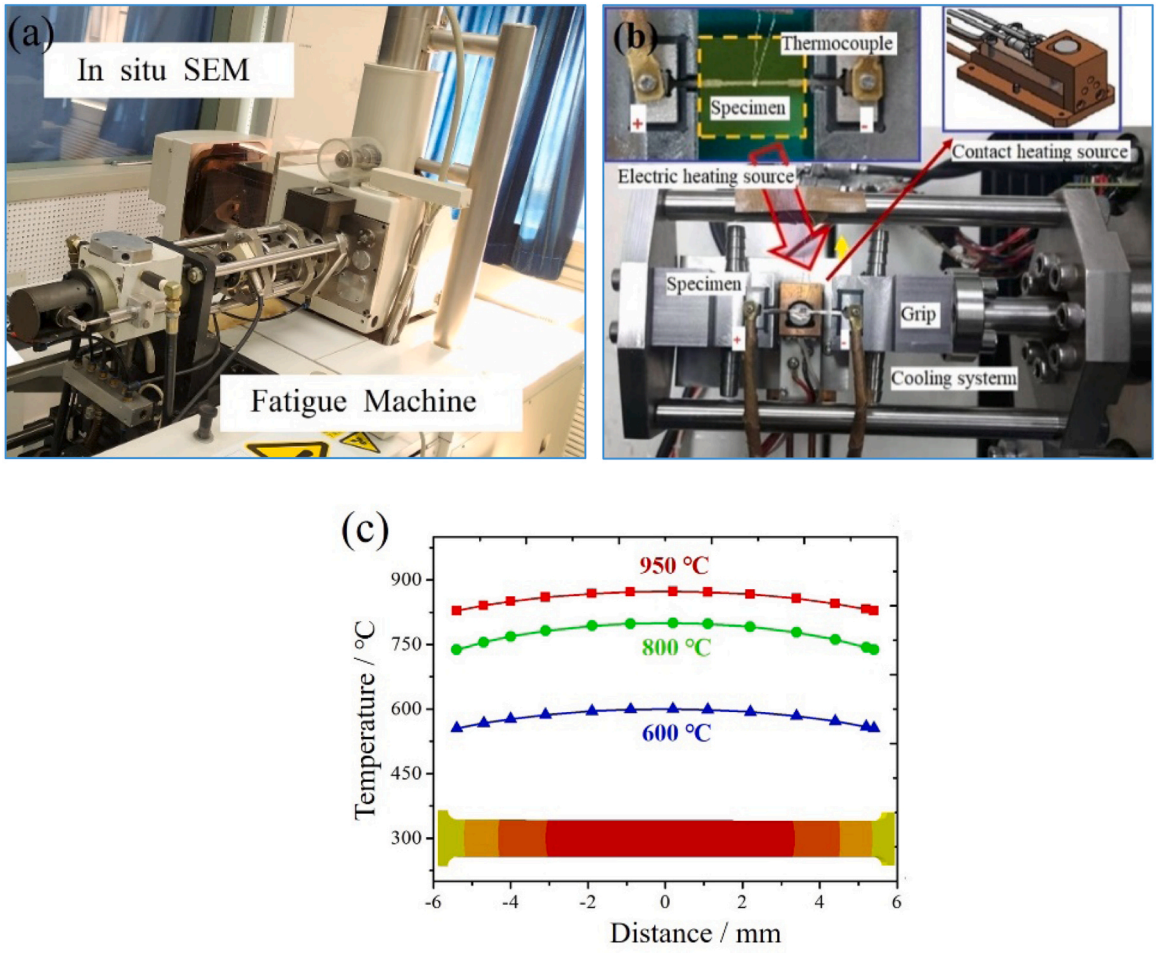


**Fig. 3.** (a) In-situ SEM fatigue equipment, (b) custom-built heating platform by contact and electric current heating, (c) temperature distribution in the intercepted section of the test specimen.

shown in Fig. 4(c). This abnormal phenomenon was similar to most nickel-based superalloys [12], which corresponded to the $L1_2$ crystal structure of the γ′ phase (discussed in detail in Section 4.1). However, the yield stress under electric heating was similar with that under contact heating from room temperature to 700 °C. When the temperature was greater than 700 °C, the yield stress decreased substantially with increasing temperature, and there was no abnormal behavior between 700 °C and 800 °C. In conclusion, when the temperature was greater than 700 °C, the yield stress of the NBSC superalloy depended on the heating method. Fig. 4(d) shows the fracture strength curves with increasing temperature under the two heating modes. For contact heating, the fracture strength hardly changed with temperature from room temperature to 700 °C. However, when the temperature was greater than 700 °C, the fracture strength decreased substantially. For electric heating, the fracture strength decreased continuously and rapidly with increasing temperature, and the downward trend was much greater than that of contact heating. Similarly to the dependence of the yield stress on the heating method, the dependence of the fracture strength was more significant.

### 3.2. Fracture analysis and characterization

The experimental results in Section 3.1 indicated that the heating mode had little effect on the elastic modulus in the elastic stage, but had an adverse effect on the yield stress and fracture strength in the plastic stage. Here, the similarities and differences of the fracture morphologies of the specimens were analyzed under the two heating methods. A large number of studies had shown that the fracture modes of NBSC superalloys usually included crystallographic fracture and non-crystallographic fracture [16,19]. Crystallographic fracture was usually along the octahedral slip plane at low and medium temperatures, which was a type of cleavage fracture. However, the path of non-crystallographic fracture did not follow the crystallographic slip surface in the high-temperature region.

Fig. 5 shows the fracture morphologies and specimen surface near fracture under the two heating modes. The fracture surface was along the different slip planes of octahedral slip system, and the slip planes and their indices had been shown in the sketch of the Fig. 5(a), (b), and (d). The high-resolution insets of fracture surface indicated that the fracture surfaces were relatively plain, which was a cleavage fracture along octahedral slip planes. In addition, there were a large number of slip lines on the specimen surface. These slip lines also meant that the potential cracking of NBSC superalloys was along the octahedral slip surface. Therefore, the NBSC superalloys showed crystallographic fracture mode when heated to 800 °C by contact heating and 600 °C by electrical heating. However, Fig. 5(c) displays that the fracture path of the NBSC superalloy was not along the octahedral slip surface at the 950 °C under the contact heating. The inset indicated that the fracture surface contained some shallow dimples, and some microvoids were evident on the specimen surface near the fracture path. Therefore, NBSC superalloys could be confirmed as non-crystallographic mode by fracture surface and path.

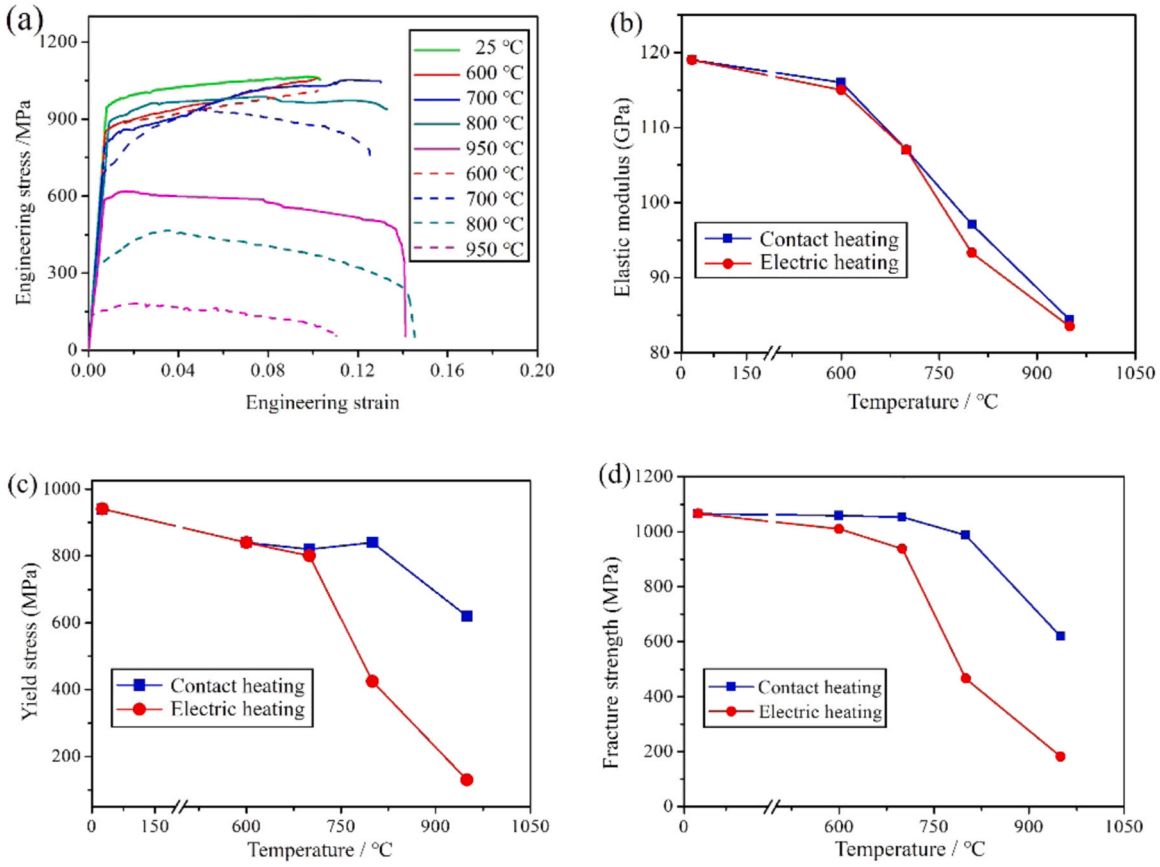


**Fig. 4.** Comparison of tensile mechanical properties of NBSC superalloy under contact and electrical heating: (a) engineering stress–strain curves (soild line: contact heating, dash line: electric heating); (b) elastic modulus; (c) yield stress; (d) fracture strength.

The fracture mode changed with temperature, which was consistent with the literature [12].

Fig. 5(e)-(f) give fracture morphologies and specimen surface near fracture under electric heating at 800 °C and 950 °C. Compared with the fracture surfaces at 600 °C, the Fig. 5(e)-(f) do not show cleavage cracking along the octahedral slip planes. It could be seen that the fracture surfaces were like a rugged ridge, but the surfaces were very smooth and exhibited a metallic luster. In addition, there were a large number of microcracks and micropores on the specimen surface near the fracture path in the insets of Fig. 5(e)-(f). The width of specimen surface near the fracture decreased, which could prove that the NBSC superalloys had the significant necking phenomenon at 800 °C and 950 °C. Holes, cracks and necking would reduce the effective cross-sectional area of the specimen and increase the current density on the cross-section. The high electric current density caused the local temperature to rise and the strength of materials to decrease. When the temperature reached the melting point in local area, the NBSC superalloys would melt. Under the action of external load, the specimens finally fractured. At this time, the joule heat effect disappears. Because the electric heating was a self-heating method, the deformation and fracture of the specimen affected the heating effect. So, its morphology at high temperature was different from that of contact heating at 950 °C.

### 3.3. Dislocation microstructure at various temperatures

Numerous studies had shown that the generation and evolution of dislocations in NBSC superalloys differed at different temperatures [2,33], resulting in different macroscopic high-temperature mechanical properties, as shown in Fig. 4. In the present experiments, the dislocation microstructures of the failed specimens at various temperatures are shown in Fig. 6, using zone axis = [1,0,0]. Regarding contact heating, at the 600 °C, the specimen was mainly manifested as two $a/2 < 011 >$ dislocation pair coupling APB that cut the $\gamma'$ phase. Eq. (1) shows the dislocation reaction mechanism [14,31]. There were also some dislocation entanglements that hindered the continuous movement of dislocations in the $\gamma$ phase. At the 800 °C, there was no dislocation pair coupling APB that cut the $\gamma'$ phase and some dislocations moved and bowed out in the $\gamma$ channel in Fig. 6(b). Moreover, the main manifestation in the $\gamma'$ phase was that the dislocations cut the $\gamma'$ phase in the form of SFs. Eq. (2) shows the dislocation reaction mechanism [14,31]. In addition, parallel dislocations were evident in some of the $\gamma'$ phase. When the temperature reached 950 °C, the quantity of SFs in the $\gamma'$ phase decreased, and dislocation loops and dislocation cross-slip phenomena were also evident in Fig. 6(c). The dislocation climbing corresponds to the relatively high temperature, which was also one of the main means of dislocation movement in NBSC superalloy at this temperature [2,3,11].

$$a/2 < 011 > + a/2 < 011 > \rightarrow a/2 < 011 > + \mathrm{APB} + a/2 < 011 > \text{ in } \gamma' \quad (1)$$

$$a/2 < 011 > \rightarrow a/3 < 121 > + a/6 < 112 > + SF \text{ in } \gamma' \quad (2)$$

However, compared with the dislocation morphologies under contact heating at the same temperature, the dislocation motion characteristics under electrical heating were quite different [22,34]. Fig. 6(d)-(f) show the dislocation morphologies of the failed specimens under a direct current power supply with feedback is used to heat the specimens. At the 600 °C, the dislocation pair coupling APB that cuts the $\gamma'$ phase remains dominant in Fig. 6(d). There was dislocation entanglement in the $\gamma$ channel, which was similar to the

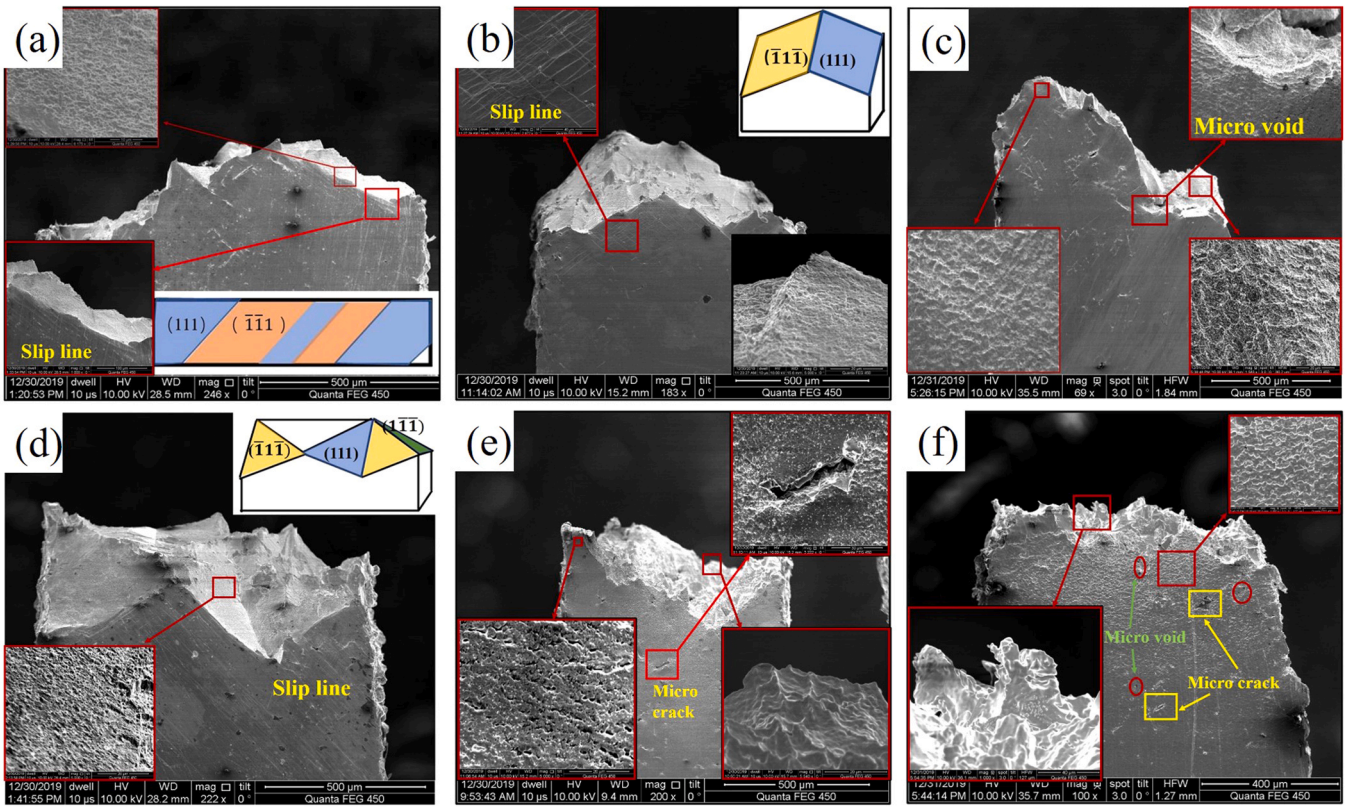


**Fig. 5.** Fracture morphologies and specimen surface near fracture at (a) 600 °C, (b) 800 °C, (c) 950 °C under contact heating; and (d) 600 °C, (e) 800 °C, (f) 950 °C under electric heating.

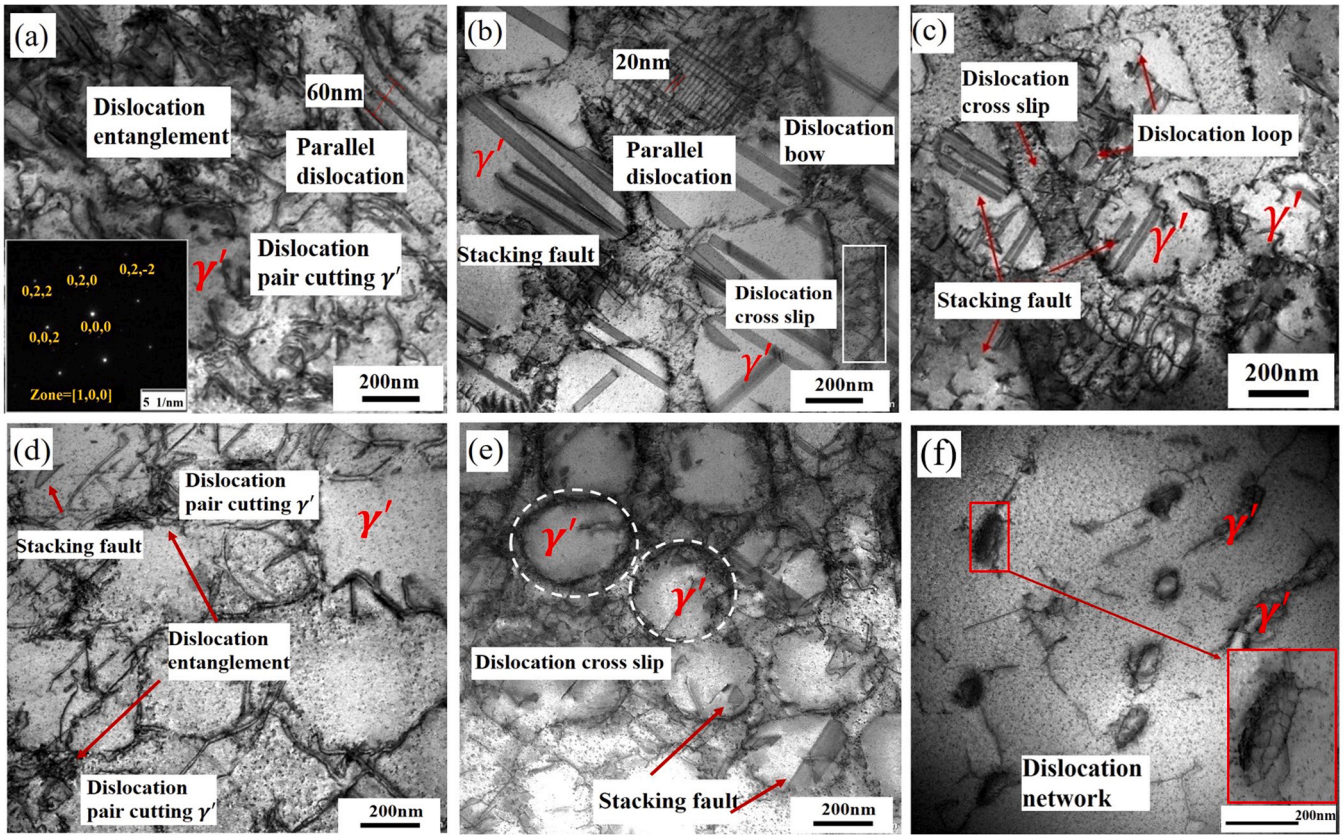


**Fig. 6.** Dislocation microstructure morphologies under contact heating at the following temperatures: (a) 600 °C, (b) 800 °C, (c) 950 °C; under electric heating at the following temperatures: (d) 600 °C, (e) 800 °C, (f) 950 °C.

deformation mechanism in Fig. 6(a). Moreover, the dislocation density was slightly lower than that in the Fig. 6(a). At 800 °C, compared with the morphology of γ′ phase in the Fig. 6(b), the rapid dissolution of the γ′ phase led to its evolution from a cubic to spherical shape, but the size did not decrease substantially. The rounding phenomenon of solidified structure for nickel base superalloys under the direct current had been reported in other studies [35]. The dislocations were mainly manifested as cross-slip movement within the γ channel and cut the γ′ phase in the form of SFs, but its density was much lower than that in Fig. 6(b). When the temperature was further heated to 950 °C, the γ′ phase dissolved substantially and its shape was tens of nanometers and spherical or ellipsoidal shape. Dislocation networks formed in the undissolved parts of the γ′ phases, which hindered further movement of the dislocation lines.

By comparing the dislocation morphologies under the two heating methods, one could conclude that the difference in the dislocation evolution gradually increased with increasing temperature. Moreover, under electric heating, the dissolution rate of the γ′ phase is substantially improved. The additional effect of the electric current on the dislocation movement cannot be ignored at medium and high temperatures for the NBSC superalloys, which will be discussed in detail in Section 4.2.

### 3.4. Elemental analysis

In accordance with the changes in the elastic modulus in Section 3.1 and the morphology of the γ′ phase in Section 3.3, one could hypothesize that the γ′ phase might have mostly dissolved at high temperature. Particularly, the change of the γ′ phase at 800 °C and 950 °C was more obvious under electric heating. The morphology change of the γ′ phase corresponded to the migration and diffusion of the elements. For NBSC superalloy, rafting of the γ′ phase often occurred in the second stage of high-temperature creep, which was mainly because of the directional diffusion of the elements [36]. The applied stress and the lattice misfit between the two phases controlled the directional diffusion [37]. The diffusion rate corresponded to the absolute temperature $T$ and the effective activation energy $Q$, which could be characterized by

$$D = D_0 \exp\left(-\frac{Q}{kT}\right) \tag{3}$$

where $D_0$ is the pre-exponential coefficient. In general, as the temperature increased, the diffusion rate of the element gradually increased. The mole fraction of the composition in the failed specimen depended on its diffusion rate and exposure time. However, because of its short exposure time at high temperature for tensile testing, the size change of the γ′ phase was not obvious under contact heating. The elemental maps in Fig. 7(a)-(c) indicate that the intensity of the element content of the γ′ phase was substantially reduced. In addition, the contents of Al, Ti, and Ta in the γ and γ′ phase are quantitatively characterized by TEM–EDS [Fig. 7(d)-(f)]. Under contact heating, the contents of Al, Ti and Ta element in the γ phase increased with increasing temperature. However, there was no obvious reduction in the γ′ phase. Under electric heating in the Fig. 7(a)-(c)], the shape of γ′ phase gradually changed from cubic to spherical with increasing temperature, and finally became small-diameter spheres or strips when the temperature reached 950 °C. Thus, the elemental diffusion rate under electric heating was greater than that under contact heating. The mole fractions of Al, Ti, and Ta in the γ phase under electric heating were much higher than those under contact heating at 800 °C and 950 °C in Fig. 7(d)-(f).

For the NBSC superalloy, Cr and Co were mainly concentrated in the γ phase and element distribution of specimen after failure was characterized by TEM-EDS. Fig. 8 displays that the elemental contents in the two phases had barely changed from room temperature to 600 °C. However, the content of Cr and Co in the γ phase decreased substantially at 800 °C and 950 °C, and their reduction ratio under electric heating was far greater than that of contact heating at the same temperature. Although the Cr and Co elements diffused from the γ phase into the γ′ phase, it did not cause a significant increase in the fraction of γ′ phase, which was shown by the blue line in the Fig. 8(d)-(e). The reason was that the volume fraction of γ′ phase of NBSC superalloy was higher than that of γ phase [38], so the total amount of Cr and Co diffusion during high-temperature tensile process was not enough to cause a significant increase of fraction in γ′ phase. For the Ni element in the two phases, it also diffused from the γ′ phase to the γ phase under both heating modes. This was mainly because the content of Ni element in the γ′ phase was higher than that in the γ phase at initial state, as shown in Table 2. It could be seen from Fig. 8(c) that the two-phase structure could not be clearly distinguished by the EDS intensity distribution of Ni element at the 950 °C under contact heating, and it could not also be distinguished at both 800 °C and 950 °C under electric heating. It could be inferred that in addition to the stress and thermal effect, the athermal effect of electric current also played an important role in the element diffusion rate.

## 4. Analysis and discussion

### 4.1. Dislocation mechanisms of yield behavior under two heating modes

From Fig. 4(c) in Section 3.1, it could be seen that with the increase of temperature, the yield stress under the two heating modes was significantly different. For contact heating, the yield stress increased significantly at 800 °C; However, for electric heating, the yield stress continued to decrease, and the degree of decline was greater than that of contact heating. Combined with the dislocation morphology in Section 3.3, the deformation mechanism of yield behavior under two heating modes would be discussed in detail in this section.

The yield behavior of materials was closely related to the initial movement behavior of dislocations. For the NBSC superalloys, the minimum resolved shear stress, $\tau$, could be used to characterize the critical value of preferential dislocation movement. Based on the dislocation movement types at different temperatures given in Section 3.3, the variations curve between the $\tau$ and temperatures were calculated and plotted in Fig. 9. The detailed calculation process is shown in Appendix A. In the low-temperature region, the resolved shear stress $\tau_{CL}$ was the smallest, so dislocation pair coupling APB that cut the γ′ phase controlled the behavior of the yield stress of the superalloy, which was consistent with the dominant dislocation morphology. In the high-temperature region, $\tau_{CL}$ was much lower than the other resolved shear stresses, and decreased with increasing temperature. Thus, the yield stress in the high-temperature region decreased substantially and continuously with temperatures. In the medium-temperature region, $\tau_{SF}$ was less than $\tau_{APB}$, which caused that a large number of SFs were evident in Fig. 6(b). Nevertheless, due to the $L1_2$ crystal structure of γ′ phase, some strengthening mechanisms appeared in the middle-temperature region, which resulted in an abnormal increase of yield stress. Because of the formation of the KW lock, the cross-slip dislocation did not readily move further [15,39]. As a result, the resolved shear stress $\tau_{KW}$ increased with the temperature in the middle-temperature region which was shown in Fig. 9. In addition, another strengthening mechanism also appeared in the present experiments, which had been reported by the authors [2]. A dislocation reaction occurred between the stacking faults I and II, as shown in Fig. 10. If two slip planes {111} intersect, a dislocation reaction might occur at the intersection line when two different a/3 < 121 > dislocations meet at the line. A fixed plane-cross dislocation configuration

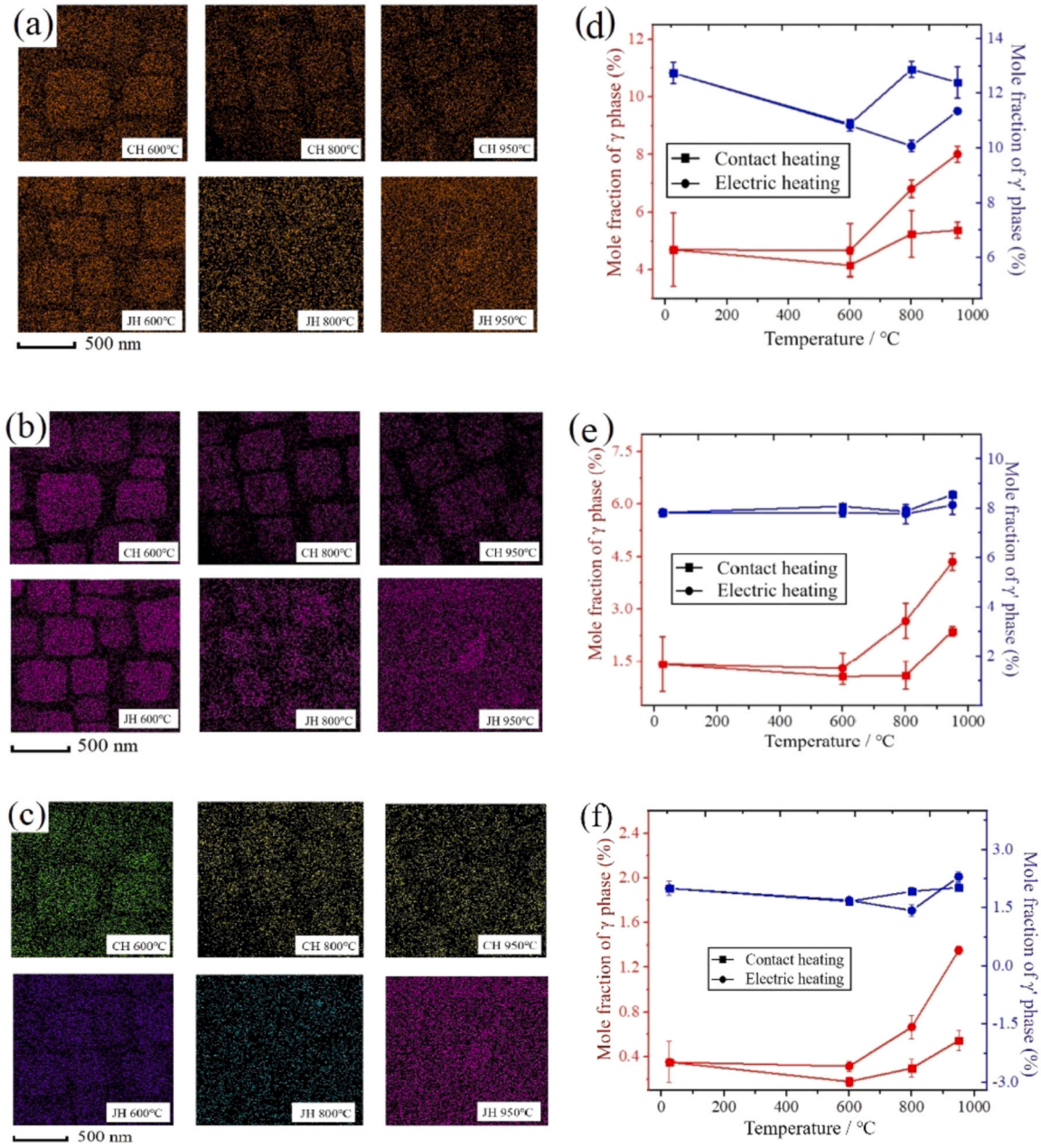


**Fig. 7.** Under contact and electric heating, TEM–EDS mapping of the following at various temperatures: (a) Al, (b) Ti, (c) Ta. Mole fraction of the following in the two phases in accordance with temperature: (d) Al, (e) Ti, (f) Ta.

formed, termed a quasi Lomer–Cottrell lock [Fig. 10(b)]. If two a/3 < 121 > dislocations did not meet or glide on two parallel {111} slip planes, the dislocations were not pertinent to strengthening [Fig. 10(c)].

Under the electric heating, the NBSC superalloy did not exhibit the abnormal behavior of the yield stress in the medium-temperature region. Obviously, this result was related to the heating mode of electric current [22,25]. By comparing Figs. 6(b) and 6(e), the phenomenon of an a/2 < 110 > dislocation that cuts the γ′ phase in the form of SFs was substantially reduced and the fixed plane-cross dislocation configuration almost disappeared at 800 °C. The unlocking stress of the KW lock also was reduced due to the athermal effect of the electric current. Previous study had confirmed that an electron wind force drives electrons in a manner that facilitates collision with the dislocation, and in so doing reduce the unlocking external stress of the KW lock [40]. All in all, the gradual fading of two dislocation strengthening mechanisms led to the disappearance of abnormal behavior yield of stress in the medium-temperature region under electric heating.

Furthermore, with increasing temperature under electric heating (also termed the current density), the yield stress and fracture strength tended to decrease more substantially compared with the same temperature under contact heating, as shown in Figs. 4(d) and 4(e). When one applied electric current to heat the specimen NBSC superalloy, the electronic wind force would promote the dislocation slip, which reduced the external force that was required for dislocation activation and movement. Under the action of an electric current, the external force that was required for dislocation movement per unit length $F/L$ is [40,41].

$$\frac{F}{L} = \frac{2Gb}{K}\exp\left(-2\pi a/Kb\right) - \alpha b P_F j/e \tag{4}$$

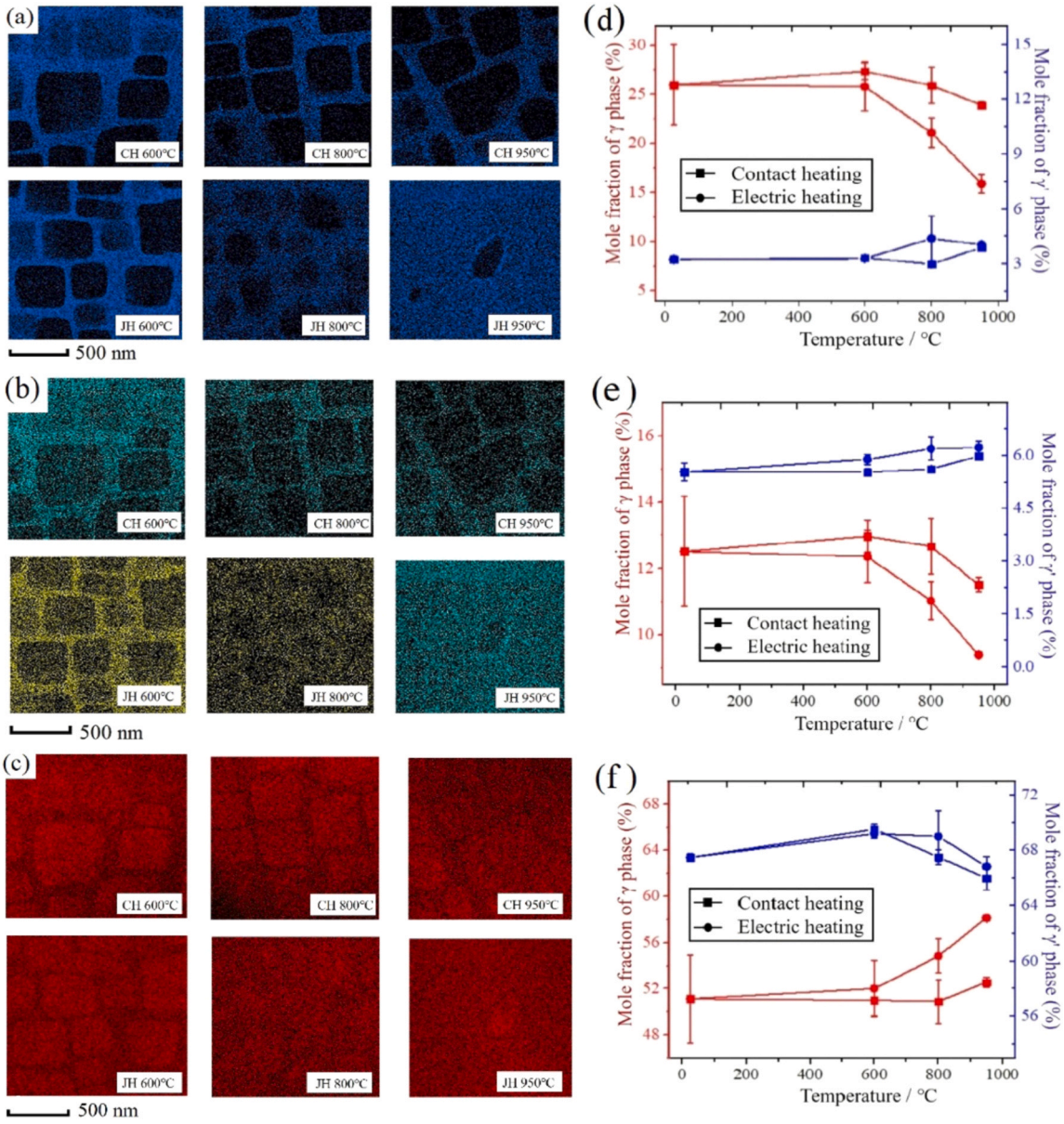


**Fig. 8.** Under the contact and electric heating, TEM–EDS mapping of the following at various temperatures: (a) Cr, (b) Co, (c) Ni. Mole fraction of the following elements in the two phases in accordance with temperature: (d) Cr, (e), Co, (f) Ni.

where $\alpha$ is 0.33, $K$ is a constant, $a$ is the interatomic spacing, $e$ is the electron charge, and $P_F$ is the Fermi momentum. Eq. (4) indicated that the external force required for dislocation movement decreased substantially with increasing current density $j$. When the specimen was heated to the nominal high-temperature region by an electric current, higher current density, $j$, would lead to dislocation climb more easily, which was also closely related to the diffusion of elements (refer to Section 4.2.1 for details).

### 4.2. Electric effect analysis

#### 4.2.1. Composition diffusion analysis

Section 3.4 revealed that the atomic diffusion increased gradually with increasing the temperature. In the high-temperature region, the diffusion rate under electric heating was higher than that under contact heating. The essence of element diffusion is the migration behavior of atoms. The driving forces of atomic migration in alloys mainly include the gradients in the atomic concentration, stress, temperature, and the electronic wind force [42]. For contact heating, the temperature distribution of the specimen was uniform after a period of heating, so the driving force for the atomic migration mainly originated from the gradients in the atomic concentration and stress. The atomic concentration mainly related to the different mole fractions of the two-phase elements in initial state, as shown in Table 2. The stress gradient mainly pertains to the difference in the thermal expansion coefficient between the two phases, the inclusion and matrix at high temperature, the lattice misfit of the $\gamma/\gamma'$ interface, and the external force. Furthermore, the higher the temperature, the more intense the atomic vibration, which will lead to a greater driving force for atomic migration. Therefore, the diffusion behaviour was enhanced with increasing temperature.

However, besides the driving forces under contact heating, the temperature gradient and electronic wind force are also essential under electric heating. For electric heating, the generation of temperature could be related to joule heating. Previous studies had shown that material resistance was affected by the electron scattering in defects. For the defect-free lattice, scattering coefficient was equal to zero [43]. For the deformed NBSC superalloys, a large

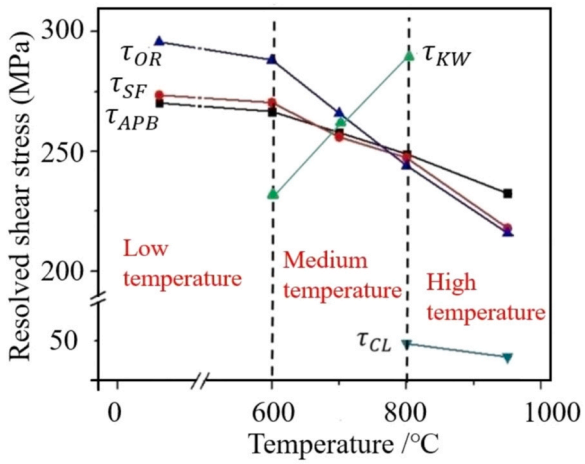


**Fig. 9.** Variations of the minimal resolved shear stresses (which correspond with five dislocation operation mechanisms) in accordance with temperature.

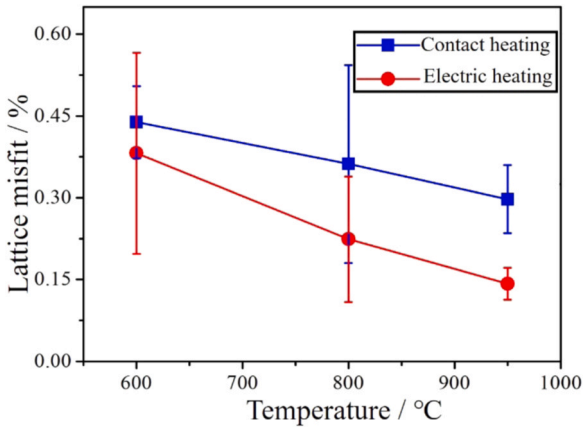


**Fig. 11.** Variation curve of the lattice misfit with temperature under the two heating modes.

number of dislocation defects would produce in critical areas, so the scattering coefficient would not be zero, resulting in large resistance in local areas. When the deformation was further increased, the NBSC superalloys would slide along slip planes and form a lot of slip bands, which would increase the electrical resistance at the slip zone. Zhang et al. confirmed that the local joule heating effect led to higher temperature in the specimen due to the local non-uniform deformation [22]. In addition, casting holes, nonmetallic inclusions, and microcracks of the tested specimens are also pertinent to temperature localization (discussed in detail in Section 4.2.2). Therefore, the temperature gradient in the specimen came from the generation of local high temperature. The electron wind force is also one of the reasons for facilitated atomic migration [44], which mainly originates from the momentum exchange between the nucleus and electrons, and the influence of the Coulomb force. With the increase of the current density, the electronic wind force increases, which promotes the ability of elemental diffusion. On the whole, the diffusion rate of electric heating was greater than that of contact heating. And this trend increased with the increase of temperature.

The morphology of the γ′ phase was affected by the elastic strain energy and γ′/γ interface energy. The elastic strain energy mainly pertains to the lattice misfit between the two phases [45]. The lattice misfit, $\delta$, is defined as:

$$\delta = 2 \times \left[ \frac{a_{\gamma'} - a_{\gamma}}{a_{\gamma'} + a_{\gamma}} \right] \tag{5}$$

where $a_{\gamma}$ and $a_{\gamma'}$ are the lattice constants of the γ and γ′ phases, respectively. In accordance with Vegard's law [1], the lattice constants of the two phases can be expressed as $a_{\gamma} = a_{\gamma}^{0} + \sum_i V_i^{\gamma} C_i^{\gamma}$ and $a_{\gamma'} = a_{\gamma'}^{0} + \sum_i V_i^{\gamma'} C_i^{\gamma'}$. $V_i^{\gamma}$ and $V_i^{\gamma'}$ are Vegard coefficients [46]. Thus, the lattice parameters are pertinent to the mole fractions of the added solutes. Combined with the mole fractions of the elements in the failed specimen in Section 3.4, we could calculate the lattice misfit $\delta$, plotted in accordance with the temperature in Fig. 11. The lattice misfit decreased gradually from 600 °C to 950 °C. The decreasing trend was more substantial under electric heating, which indicates that there was less elastic strain energy between the two phases in the tensile process. When the size of the γ′ phase was small and the elastic strain energy was low, the morphology of the γ′ phase would be mainly controlled by the interfacial energy. In the process of elemental diffusion, when the shape of the γ′ phase remains spherical, this phase had the lowest interface energy [47,48]. Therefore, in the process of electric heating, the γ′ phase shape of the failed specimen became spherical with increasing temperature.

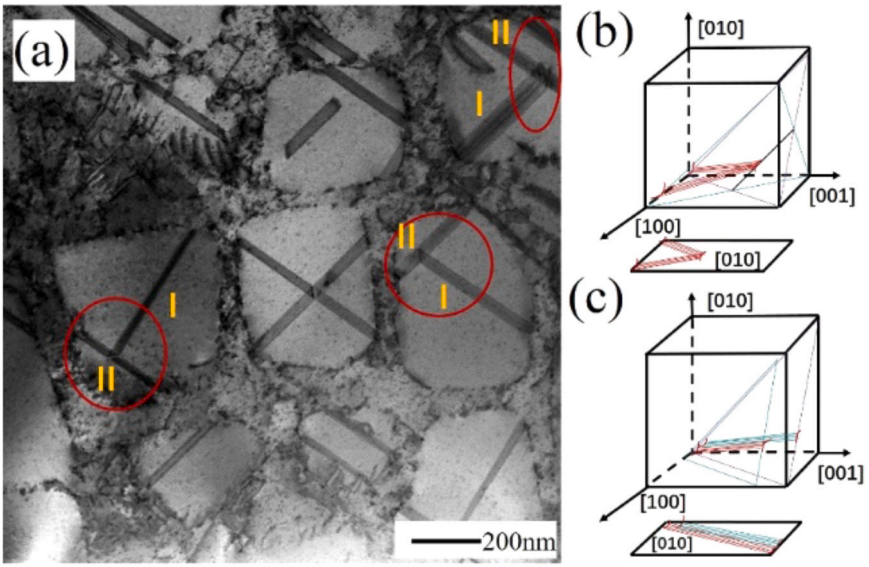


**Fig. 10.** (a) Dislocation morphology at 800 °C. Schematics of the following: (b) dislocation gliding on two intersecting {111} planes, (c) dislocation slip on two parallel {111} planes.

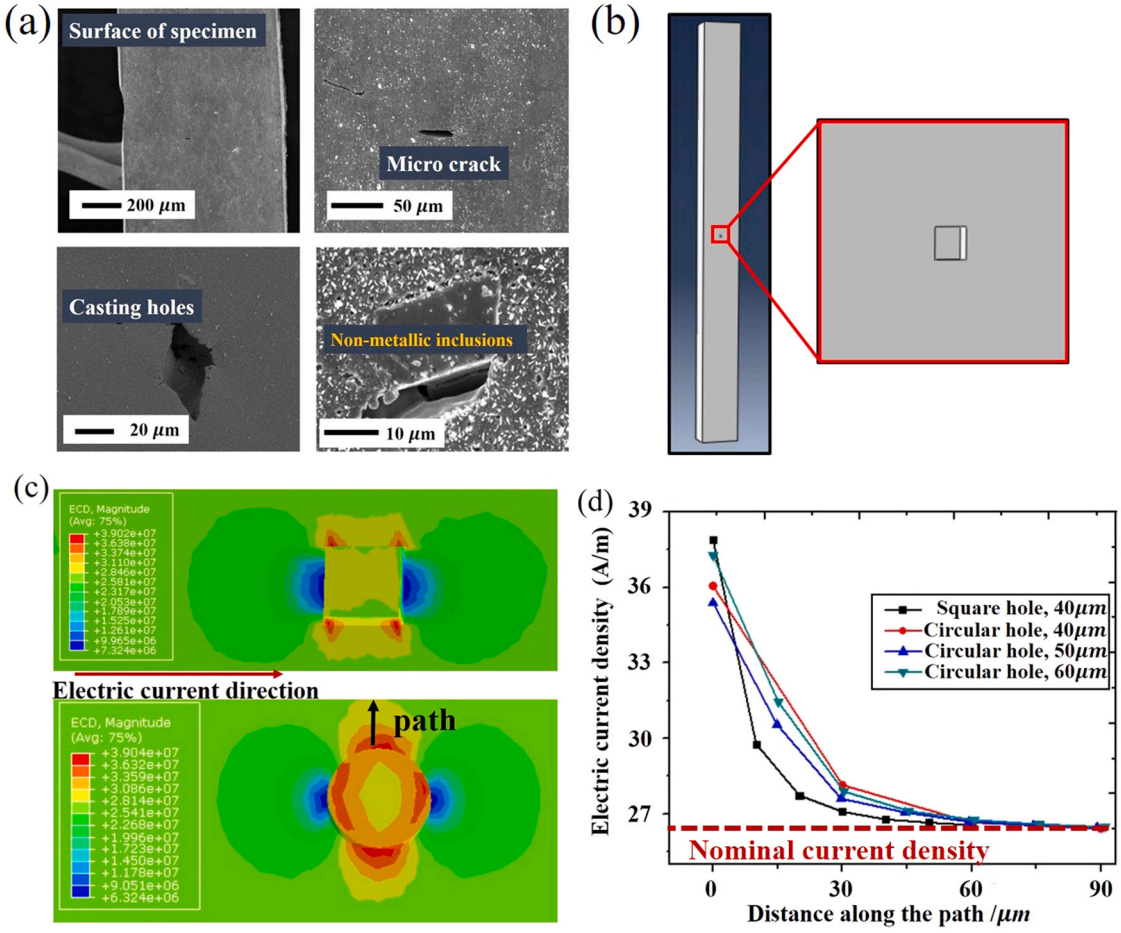


**Fig. 12.** (a) Casting defect of the NBSC superalloy, (b) thermal–electric coupling of the finite-element model, (c) distribution map of the electric current density under various shape defects, (d) current density variation along the direction of the path (marked with a black arrow in part c).

*4.2.2. Effect of holes or nonmetallic inclusions on electric heating*

Regarding contact heating, the size of the heat source was much larger than the width of the specimen. Thus, the temperature of the tested zone of the specimen was uniform. However, under electric heating, the specimen undergone self-heating through the Joule heating effect. The nonuniformity of materials in the casting process might further cause a nonuniformity in the temperature distribution and electric current density. Generally, the microstructure defects in NBSC superalloy mainly include pores and nonmetallic inclusions [Fig. 12(a)]. Because these two types of defects were nonconductive, an electrical current did not pass through them. To characterize the influence of defects on electric heating, finite-element analysis was carried out by adopting a thermal–electric coupling model. The simulation parameters were the same as those in Section 2.2. Generally, the size of the pores and nonmetallic inclusions ranged from a few micronmeters to tens of micronmeters. Fig. 12(b) showed the established finite-element model. The boundary condition was to apply the voltage difference at both ends of the specimen, and the element was DC3D8E-type. Fig. 12(c) shows the simulation results.

The electric current density on both sides of the defect along the current direction was low, whereas it increased on both sides perpendicular to the current direction [Fig. 12(c)]. Fig. 12(d) showed the current density variation along the direction of the vertical path. As the distance from the defect increased in the vertical direction, the electric current density gradually tended to the nominal current density. In accordance with Joule theory [22,49], one can express the temperature increase $\Delta T$ as $\Delta T = j^2 \rho V \Delta t/(mc)$, where $\rho$ is the electrical resistivity, $V$ and $m$ are the volume and mass of the conductive part, and $c$ is the specific heat capacity, respectively. Thus, the temperature in this region was higher than in the nominal temperature of the specimen. Therefore, under electric heating, the locally high temperature caused by Joule heating (induced by pores or nonmetallic inclusions) was another factor that contributed to the deterioration in the mechanical properties of the NBSC superalloy.

## 5. Conclusions

Combined with the self-designed contact and electric heating methods, tensile experiments of a NBSC superalloy from room temperature to 950 °C were conducted by an in-situ SEM high-temperature platform. We demonstrated that the similarities and differences of mechanical properties of NBSC superalloys under two heating modes are closely related to its temperature. Based on the present experimental results and theoretical analysis, the main conclusions are as follows:

- The mechanical properties exhibit little difference under the contact heating and the electric heating with temperature below 600 ℃, while for temperature above 600 ℃, the tensile mechanical properties of the NBSC superalloy (such as the yield stress and fracture strength) decrease more rapidly under the electric heating. The fracture morphology, dislocation microstructure, and composition distribution also support this finding.
- Under contact heating, the yield stress increases with increasing temperature in the low- to high-temperature range, whereas the abnormal behavior is found in the medium-temperature range,

mainly controls by the KW lock and quasi-Lomer–Cottrell lock. Based on the dominant dislocation deformation mechanism, a correlation between the dislocation deformation and the critical shear stress is characterized under different temperature.

- Under electric heating, when the temperature exceeds 600 °C, the tensile mechanical properties of the NBSC superalloy (such as the yield stress and fracture strength) decreased rapidly, which is mainly corresponds to the local Joule heat effect and athermal effect of the current. The electric current acts on the dislocation line, causing the dislocation to glide more easily.
- With increasing temperature, the diffusion rate of the NBSC superalloy increased gradually. In contact heating, the driving force mainly originates from the gradients in the atomic concentration and stress. In electric heating, the effects of temperature gradient and electronic wind force are also included. The temperature gradient mainly originates from the local Joule heat effect, mainly caused by defects such as dislocations, holes, and nonmetallic inclusions. Therefore, a relatively large driving force leads to its strong diffusion in contrast to that of contact heating. In addition, the γ′ phase changes from cubic to spherical shape because of the large diffusion rate under electric heating, which is mainly affected by the lattice misfit.

## CRediT authorship contribution statement

**Zhen Wang:** Conceptualization, Methodology, Investigation Writing – original draft, Formal analysis, Visualization, Funding acquisition. **Xingzhi Huang:** Investigation, Resources, Writing – original draft. **Xuan Ye:** Conceptualization, Funding acquisition, **Chong Zhao:** Visualization, Writing – review & editing. **Jianqiao Hu:** Writing – review & editing. **Zhigang Li:** Data curation, **Xiaoming Liu:** Writing – review & editing. **Xide Li:** Conceptualization, Supervision, Funding acquisition.

## Data Availability

Data will be made available on request.

## Declaration of Competing Interest

The authors declare that they have no known competing financial interests or personal relationships that could have appeared to influence the work reported in this paper.

## Acknowledgments

This work was financially supported by the National Natural Science Foundation of China (grant numbers 11632010, 11872035, 12272203, 12202450, 12172190) and National Science and Technology Major Project (J2019-VI-0002-0115).

## Appendix A. the minimum critical shear stress of five dislocation deformation mechanisms

Based on the experimental results of Section 3.3, the types of dislocation movement in the NBSC superalloy mainly included: dislocation pair coupling APB that cut the γ′ phase, dislocation cutting γ′ phase in the form of SFs, dislocation bypassed the γ′ phase in the form of bowing and climbing. In addition, when dislocations moved in cross slip in the middle-temperature region, the formation of KW lock would hinder the further movement of dislocations, so KW lock was also an important dislocation mechanism [39]. The minimum critical shear stress, $\tau$ of five dislocation deformation mechanisms were calculated:

The shear phenomenon of dislocation that cuts the γ′ phase was given by [13].

$$\tau_{\mathrm{APB}} = 1.02\frac{Gbwf^{0.5}}{\pi d}\left(1+\frac{Cf^{0.5}}{2}\right)\sqrt{\frac{\pi d\gamma_{\mathrm{APB}}}{wGb^2}-1} \tag{A1}$$

$$\tau_{\mathrm{SF}} = \sqrt{3}\left(\frac{G(2-\nu)}{12(1-\nu)}\frac{\pi b}{2d}+\frac{2\gamma_{\mathrm{SF}}}{3b}\right) \tag{A2}$$

The shear stress, $\tau$, for dislocation bypass mechanism could express the Orowan stress [50] and dislocation climbing stress [51] by Eqs. (A3) and (A4), respectively

$$\tau_{\mathrm{OR}} = \sqrt{\frac{2}{3}}\frac{Gb}{h} \tag{A3}$$

$$\tau_{\mathrm{CL}} = f^{1.5}\tau_{\mathrm{OR}}/2^{1.25} \tag{A4}$$

where $\tau_{APB}$, $\tau_{SF}$, $\tau_{OR}$, and $\tau_{CL}$ represented the minimal resolved shear stress required for the four dislocation mechanisms to occur, respectively. $G$ = 51.7–75.3 GPa is the shear modulus of NBSC superalloy in the {111} direction, $\nu$ = 0.32 is the Poisson's ratio, $f$ = 80% is the volume fraction of the γ′ phase [38], $d$ = 340.12 nm is the average diameter of the γ′ phase, $h$ = 52.00 nm is the average width of the γ channel, $b$ = 0.25 nm is the Burgers vector of the a/2 < 011 > dislocation. $w$ and $C$ are constants, usually $w$ = 2.8 and $C$ = 1 [52]. $\gamma_{\mathrm{APB}}$ and $\gamma_{\mathrm{SF}}$ are the APB and SF energies, respectively, which are measured experimentally. Ru et al. [53] had confirmed that the APB energy, $\gamma_{APB}$, and the mole fraction of element $i$ in the γ′ phase, $C_i^{\gamma'}$, were linearly correlated, and given by

$$\gamma_{\mathrm{APB}} = \gamma^0_{\mathrm{APB}} + 137.6C^{\gamma'}_{\mathrm{Co}} + 239.6C^{\gamma'}_{\mathrm{Cr}} + 269.0C^{\gamma'}_{\mathrm{Mo}} + 270.5C^{\gamma'}_{\mathrm{Ta}} + 235.3C^{\gamma'}_{\mathrm{Ti}} + 276.8C^{\gamma'}_{\mathrm{W}} \tag{A5}$$

where $\gamma^0_{\mathrm{APB}}$ = 182 mJ/m$^2$ is the APB energy of $Ni_3Al$. Kim et al. [54] estimated the SF energy by

$$\gamma_{\mathrm{SF}} = \Gamma_{\mathrm{Ni}}(T)\left(1+\sum C_i^{\gamma'}\delta\Gamma_i\right) \tag{A6}$$

where $\Gamma_{\mathrm{Ni}}$ $(T)$ is the SF energy of Ni, and $C_i^{\gamma'}$ is the mole fraction of element $i$ in the γ′ phase. $\delta\Gamma_i$ are different constants for the different elements and the specific values could be found in the lirerature [54]. Under contact heating, the Mole fraction of the γ′ phase at various temperatures was measured by TEM–EDS in Section 3.4.

In addition, in the medium-temperature region, the resolved shear stress that is required for the unlocking of the KW lock are determined by [55].

$$\tau_{KW} = 8.25\frac{l_c}{b} + 50 \tag{A7}$$

where $l_c$ is the formation height of the KW lock. The height corresponded to the temperature [56]. At a specific temperature, one can determine the average height $l_c$ by

$$l_c = d_c \exp\left(\frac{-W_c}{kT}\right) \tag{A8}$$

where $d_c = 80b$, $W_c = 1.52 \times 10^{-20}$ J, and $k = 1.368 \times 10^{-23}$ J/K is the Boltzmann constant.

## References


[1] R.C. Reed, The Superalloy: Fundamentals and Applications, Cambridge University Press, 2006.
[2] L.Q. Cui, H.H. Su, J.J. Yu, J.L. Liu, et al., Temperature dependence of tensile properties and deformation behaviors of nickel-base superalloy M951G, Mater. Sci. Eng. A. 696 (2017) 323–330.
[3] P. Zhang, Y. Yuan, S.C. Shen, B. Li, et al., Tensile deformation mechanisms at various temperatures in a new directionally solidified Ni-base superalloy, J. Alloy. Compd. 694 (2017) 502–509.
[4] N.R. Sun, L.T. Zhang, Z.G. Li, A.D. Shan, The effect of microstructure on the creep behavior of a low rhenium-containing single crystal nickel-based superalloy, Mater. Sci. Eng. A. 606 (2014) 175–186.
[5] F. Li, Z.X. Wen, Z.Yn Wu, H.Q. Pei, Z.F. Yue, Fatigue life assessment of nickel-based single crystals considering equivalent initial flaw size model and anisotropy, Int. J. Fatigue 160 (2022) 106886.
[6] K.S. Li, J. Wang, Z.C. Fan, L.Y. Cheng, S.L. Yao, R.Z. Wang, X.C. Zhang, S.T. Tu, A life prediction method and damage assessment for creep-fatigue combined with high-low cyclic loading, Int. J. Fatigue 161 (2022) 106923.
[7] E. Stefan, S. Christoph, Characterization of fatigue crack growth damage mechanisms and damage evolution of the nickel-based superalloy MAR-M247 CC (HIP) and CM-247 LC under thermomechanical fatigue loading using in situ optical microscopy, Int. J. Fatigue 99 (2017) 235–241.
[8] X.Y. Ren, J.X. Lu, J.L. Zhou, X.Q. Liu, W.X. Jiang, J. Wang, Y.F. Zhang, Z. Zhang, In-situ fatigue behavior study of a nickel-based single-crystal superalloy with different orientations, Mater. Sci. Eng. A 855 (2022) 143913.
[9] W. Kang, I. Beniam, S.M. Qidwai, In situ electron microscopy studies of electromechanical behavior in metals at the nanoscale using a novel microdevice-based system, Rev. Sci. Instrum. 87 (2016) 095001.
[10] X.Q. Li, J. Turner, K. Bustillo, A.M. Minor, In situ transmission electron microscopy investigation of electroplasticity in single crystal nickel, Acta Mater. 223 (2022) 117461.
[11] Z.P. Luo, Z.T. Wu, D.J. Miller, The dislocation microstructure of a nickel-base single-crystal superalloy after tensile fracture, Mater. Sci. Eng. A 354 (2003) 358–368.
[12] J.J. Wang, W.G. Guo, Y. Su, P. Zhou, K.B. Yuan, Anomalous behaviors of a single-crystal Nickel-base superalloy over a wide range of temperatures and strain rates, Mech. Mater. 94 (2016) 79–90.
[13] Z.K. Chu, X.F. Sun, H.R. Guan, Z.Q. Hu, Y. Jinjiang, Tensile property and deformation behavior of a directionally solidified Ni-base superalloy, Mater. Sci. Eng. A 527 (2010) 3010–3014.
[14] X.G. Wang, J.L. Liu, T. Jin, X.F. Sun, Tensile behaviors and deformation mechanisms of a nickel-base single crystal superalloy at different temperatures, Mater. Sci. Eng. A 598 (2014) 154–161.
[15] Z.H. Tan, X.G. Wang, Y.L. Du, et al., Temperature dependence on tensile deformation mechanisms in a novel Nickel-based single crystal superalloy, Mater. Sci. Eng. A 776 (2020) 138997.
[16] Y.Y. Zhang, H.J. Shi, J.L. Gu, C.P. Li, K.D. Kai, O. Luesebrink, Crystallographic analysis for fatigue small crack growth behaviors of a nickel-based single crystal by in situ SEM observation, Theor. Appl. Fract. Mech. 69 (2014) 80–89.
[17] C.A. Sweeney, B. O'Brien, F.P.E. Dunne, P.E. McHugh, S.B. Leen, Micro-scale testing and micromechanical modelling for high cycle fatigue of CoCr stent material, J. Mech. Behav. Biomed. 46 (2015) 244–260.
[18] J.C. Liang, Z. Wang, H.F. Xie, X.D. Li, In situ scanning electron microscopy-based high-temperature deformation measurement of nickel-based single crystal superalloy up to 800℃, Opt. Laser Eng. 108 (2018) 1–14.
[19] J.C. Liang, Z. Wang, X.D. Li, In situ scanning electron microscopy analysis of effect of temperature on small fatigue crack growth behavior of nickel-based single-crystal superalloy, Int. J. Fatigue 128 (2019) 105–195.
[20] X.Z. Huang, X.D. Li, Temperature control method during current heating of a specimen in scanning micro enviroment, J. Exp. Mech. 34 (2019) 911–925.
[21] J. Liu, W.T. Tang, J.H. Li, Deformation and fracture behaviors of K403 Ni-based superalloy at elevated temperatures, J. Alloy. Compd. 699 (2017) 581–590.
[22] X. Zhang, H. Li, M. Zhan, Mechanism for the macro and micro behaviors of the Ni-based superalloy during electrically-assisted tension: local Joule heating effect, J. Alloy. Compd. 1 (2018) 325.
[23] S. Patrick, McNeff, Brian K. Paul, Electroplasticity effects in Haynes 230, J. Alloy. Compd. 829 (2020) 154438.
[24] X. Zhang, H.W. Li, S.L. Yan, N. Zhang, Experimental study and analysis on the electrically-assisted tensile behaviors of Inconel 718 alloy, Procedia Eng. 207 (2017) 365–370.
[25] K. Han, S.X. Qin, H.P. Li, J. Liu, et al., EBSD study of the effect of electropulsing treatment on the microstructure evolution in a typical cold-deformed Ni-based superalloy, Mater. Charact. 158 (2019) 109936.
[26] C. Rudolf, R. Goswami, W. Kang, J. Thomas, Effects of electric current on the plastic deformation behavior of pure copper, iron, and titanium, Acta Mater. 209 (2021) 116776.
[27] W.S. Xia, X.B. Zhao, L. Yue, Z. Zhang, A review of composition evolution in Ni-based single crystal superalloys, J. Mater. Sci. Technol. 44 (2020) 76–95.
[28] B. Roebuck, D. Cox, R. Reed, The temperature depenence of γ′ volume fraction in a Ni-based single crystal superalloy from resistivity measurements, Scr. Mater. 44 (2001) 917–921.
[29] C.M. Kenneth, Y.H.M. Youssef, Z.S. Li, Y.C. Su, Calculation of thermophysical properties of ni-based superalloy, ISIJ Int. 46 (2006) 623–632.
[30] Z. Wang, W.W. Wu, J.C. liang, X.D. Li, Creep–fatigue interaction behavior of nickel-based single crystal superalloy at high temperature by in-situ SEM observation, Int. J. Fatigue 141 (2020) 105879.
[31] Y.F. Liu, Y.S. Zhao, C.G. Liu, et al., Dependence on temperature of tensile properties of the single-crystal superalloy DD11, Mater. Sci. Technol. 34 (2018) 1188–1196.
[32] D. Siebörger, H. Knake, U. Glatzel, Temperature dependence of the elastic moduli of the nickel-base superalloy CMSX-4 and its isolated phases, Mater. Sci. Eng. A 298 (2001) 26–33.
[33] T.J. Zhou, H.S. Ding, X.P. Ma, W. Feng, H.B. Zhao, A.L. Li, Y. Meng, H.X. Zhang, Effect of precipitates on high-temperature tensile strength of a high W-content cast Ni-based superalloy, J. Alloy. Compd. 797 (2019) 486–496.
[34] S.Q. Xiang, X.F. Zhang, Dislocation structure evolution under electroplastic effect, Mater. Sci. Eng. A 761 (2019) 138026.
[35] Y.S. Yang, W.F. Li, Z.Z. Wang, Z.Q. Hu, S. Hanada, Z. Zhong, S.W. Nam, R.N. Wright, 4th Pacific Rim Int Conf on Advanced Materials and Processing Vol. 1 2001 The Japan Institute of Metals Tokyo 345.
[36] J.X. Zhang, J.C. Wang, H. Harada, Y. Koizumi, The effect of lattice misfit on the dislocation motion in superalloys during high-temperature low-stress creep, Acta Mater. 53 (2005) 4623–4633.
[37] C. He, L. Liu, T.W. Huang, W.C. Yang, X.J. Wang, J. Zhang, M. Guo, H.Z. Fu, The effects of misfit and diffusivity on γ′ rafting in Re and Ru containing Nickel based single crystal superalloy-details in thermodynamics and dynamics, Vacuum 183 (2021) 109839.
[38] O. Aslan, Numerical modeling of fatigue crack growth in single crystal nickel based superalloys, Mater. École Natl. Supér. Des. Mines De. Paris (2010).
[39] Y.M. Wang-Koh, Understanding the yield behaviour of L12-ordered alloys, Mater. Sci. Technol. 33 (2017) 943-943.
[40] S.D. Antolovich, H. Conrad, The effects of electric currents and fields on deformation in metals, ceramics, and ionic materials: an interpretive survey, Mater. Manuf. Process. 19 (2004) 587–610.
[41] J.Y. Liu, K.F. Zhang, Influence of electric current on superplastic deformation mechanism of 5083 aluminium alloy, Mater. Sci. Technol. 32 (2016) 540–547.
[42] C.M. Tan, A. Roy, Investigation of the effect of temperature and stress gradients on accelerated EM test for Cu narrow interconnects, Thin Solid Films 504 (2006) 288–293.
[43] X.W. Wang, J. Xu, Z.L. Jiang, W.L. Zhu, D.B. Shan, B. Guo, J. Cao, Size effects on flow stress behaviour during electrically-assisted micro-tension in a magnesium alloy AZ31, Mater. Sci. Eng. A 659 (2016) 215–224.
[44] V.B. Fiks, On the mechanism of the mobility of ions in metals, Sov. Phys. Solid State (1959) 1–14.
[45] J.S. Van Sluytman, T.M. Pollock, Optimal precipitate shapes in nickel-base γ–γ′ alloys, Acta Mater. 60 (2012) 1771–1783.
[46] P. Caron, High γ′ solvus new generation nickel-based superalloy for single crystal turbine blade applications, Superalloy (2000) 737–746.
[47] H.Y. Li, X.P. Song, Y.L. Wang, et al., Coarsening and age hardening behaviors of γ′ particles in GH742 during high temperature treatment, J. Iron Steel Res. Int. 16 (5) (2009) 81–86.
[48] W. Sun, X. Qin, J. Guo, et al., Microstructure stability and mechanical properties of a new low cost hot-corrosion resistant Ni-Fe-Cr based superalloy duringlong-term thermal exposure, Mater. Des. 69 (2015) 70–80.
[49] W.A. Salandro, J.J. Jones, C. Bunget, L. Mears, J.T. Roth, Electrically Assisted Forming, Springer, UK, 2015.

[50] T.M. Pollock, A.S. Argon, Creep resistance of CMSX-3 nickel based superalloy single crystals, Acta Metall. Mater. 40 (1992) 1–30.
[51] R.S.W. Shewfelt, L.M. Brown, High-temperature strength of dispersion-hardened single-crystals: theory, Philos. Mag. 35 (1977) 945–962.
[52] B. Reppich, Some new aspects concerning particle hardening mechanisms in γ′ precipitating Ni-base alloys-I theoretical concept, Acta Metall. 30 (1982) 87–94.
[53] R. Yi, Z. Haigen, Z. Heng, Design for anomalous yield in γ′-strengthening superalloy, Mater. Des. 183 (2019) 108 -082.
[54] Y.K. Kim, D. Kim, H.K. Kim, C.S. Oh, B.J. Lee, An intermediate temperature creep model for Ni-based superalloy, Int. J. Plast. 79 (2016) 153–175.
[55] D. Benoit, V. Patrick, P.K. Ladislas, S. Georges, A simulation of dislocation dynamics and of the flow stress anomaly in L12 alloys, Philos. Mag. A 75 (1997) 1263–1286.
[56] B. Devincre, P. Veyssière, G. Saada, Simulation of the plastic flow in Ni3Al: work hardening and strain-rate sensitivity, Philos. Mag. A. 79 (1999) 1609–1627.